1   *This is a non-peer-reviewed preprint*

2   High-resolution mapping of forest vulnerability to
3   wind for disturbance-aware forestry and climate
4   change adaptation

5

6   Susanne Suvanto*[1], Mikko Peltoniemi[1], Sakari Tuominen[1], Mikael Strandström[1], Aleksi
7   Lehtonen[1]

8   [1]*Natural Resources Institute Finland (Luke), Latokartanonkaari 9, 00790 Helsinki*

9   ** Corresponding author*

10   Abstract

11   Windstorms cause major disturbances in European forests and forest management can play

12   a key role in making forests more persistent to disturbances. However, better information is

13   needed to support decision making that effectively accounts for wind disturbances. Here we

14   show how empirical probability models of wind damage, combined with existing spatial

15   datasets, can be used to provide fine-scale spatial information about disturbance probability

16   over large areas. First, we created stand-level damage probability models with predictors

17   describing forest characteristics, recent forest management history and local wind, soil, site

18   and climate conditions. We tested three different methods for creating the damage

19   probability models - generalized linear models (GLM), generalized additive models (GAM)

20   and boosted regression trees (BRT). Then, the damage probability maps were calculated by

21   combining the models (GLM, GAM and BRT) with GIS data sets representing the model

22   predictors. Finally, we demonstrated the predictive performance of the maps with a large,

23   independent test data, which shows that the damage probability maps are able to identify

24   vulnerable forests also in new wind damage events (AUC > 0.7). Use of the more complex

25   methods (GAM and BRT) was not found to improve the predictive performance of the map

26   compared to GLM, and therefore we would suggest using the more simple GLM method that

27   can be more easily interpreted. The map allows identification of vulnerable forest areas in

28   high spatial resolution (16 x 16 m^2 raster resolution), making it useful in assessing the

29   vulnerability of individual forest stands when making management decisions. The map is

30   also a powerful tool for communicating disturbance risks to forest owners and managers and

31   it has the potential to steer forest management practices to a more disturbance aware

32   direction. Our study showed that in spite of the inherent stochasticity of the wind and

33   damage phenomena at all spatial scales, it can be modelled with good accuracy across

34   large spatial scales when existing ground and earth observation data sources are combined

35   smartly. With improving data quality and availability, map-based risk assessments can be

36   extended to other regions and other disturbance types.

37   **Keywords:** *forest disturbances; storm damage; windthrow; tree mortality; forest*

38   *management; climate change*

39   1. Introduction

40   Forest wind disturbances have major economic, societal and ecological consequences in

41   Europe. Forest disturbances have substantial effects on forest productivity and carbon

42   storage (Reyer et al., 2017; Seidl et al., 2014), and therefore actions to reduce and manage

43   the disturbances are crucial in assuring the persistence of the forest carbon sinks. The

44   damage caused by wind storms in European forests has increased during the past century

45   (Gregow et al., 2017; Schelhaas et al., 2003; Seidl et al., 2011) and this trend is expected to

46   continue (Ikonen et al., 2017; Seidl et al., 2017). The question of forest wind disturbances is

47   therefore becoming increasingly important in the future.

48   Forest management practices play a key role in making forests less vulnerable to wind

49   disturbances. Management driven changes in European forests, such as increasing standing

50   timber volume and promotion of conifer species, have been identified as one of the major

51   causes of increased forest disturbances in Europe during the latter half of the 20th century

52   (Schelhaas et al., 2003; Seidl et al., 2011). If management practices are shifted to reduce

53   forest vulnerability to wind, it may be possible to decrease the negative effects of wind

2

54   disturbances. However, changing the forest management practises to more disturbance-

55   aware direction is not always easy, as illustrated by the 2005 storm Gudrun in southern

56   Sweden. Despite the massive damage and economic losses caused by the storm and the

57   Swedish Forest Agency's recommendations for alternative, less vulnerable, management

58   options, the forest management practises in the area remained largely unchanged after the

59   storm (Andersson et al., 2018; Valinger et al., 2014). This demonstrates that not only is

60   information about the wind damage risks urgently needed to account for disturbances in

61   management decisions, but it is also crucial that this information is in a form that can be

62   effectively used and communicated to forest owners and managers.

63   The development of remote sensing methods and the progress of open data policies have

64   substantially increased the amount, quality and availability of spatial data relating to forests.

65   This opens new possibilities for detailed spatial estimation of forest sensitivity to

66   disturbances. Vulnerability of forests to wind damage is affected by forest characteristics,

67   forest management as well as the abiotic environment, such as local wind and soil

68   conditions (Mitchell, 2013). For example, probability of wind damage has been shown to

69   increase with tree height and certain species, such as Norway spruce, are particularly

70   vulnerable to wind (Dobbertin, 2002; Peltola et al., 1999; Valinger and Fridman, 2011).

71   Forest management has major effects on wind damage sensitivity, as trees that have grown

72   in sheltered conditions and have later been exposed to wind, because of thinning or clear cut

73   of the neighboring stand, are especially sensitive to damage (Lohmander and Helles, 1987;

74   Peltola et al., 1999; Suvanto et al., 2016). Areas that are exposed to strong wind gusts

75   (Schindler et al., 2016) or where rooting conditions are limited due to soil characteristics

76   (Nicoll et al., 2006) are more predisposed to wind damage. Therefore, in order to provide

77   useful information on forest vulnerability to wind damage, information from several different

78   sources, scales and disciplines needs to be brought together.

79   Logistic generalized linear models (GLM) have long been applied in statistical modelling of

80   forest wind damage (Lohmander and Helles, 1987; Suvanto et al., 2016; Valinger and

3

81 Fridman, 1997). In addition, different approaches allowing more flexible model behaviour

82 than fully parametric GLMs have been used, such as generalized additive models (GAM;

83 Schmidt et al., 2010) that use non-parametric smooth functions to allow more flexibility in the

84 relationship of response variable and predictors (Hastie et al., 2009). Machine learning

85 approaches have also been successfully applied to wind disturbance modeling (see

86 Hanewinkel et al. 2004 for an early example) and recently especially tree-based ensemble

87 models, such as random forests, have been shown to perform well in predicting wind

88 damage (Albrecht et al., 2019; Hart et al., 2019; Kabir et al., 2018; Schindler et al., 2016).

89 While machine learning methods and additive models are able to more flexibly fit the data

90 and account for non-linearities, the GLMs have strengths in their straightforward

91 interpretability and the robustness of predictions (Albrecht et al., 2019; Nakou et al., 2016).

92 In this study, our goal was to create high-resolution spatial information about forest

93 vulnerability to wind damage in Finland, using an extensive damage observation data set

94 and a large compilation of spatial data sources to achieve this. More specifically, we aimed

95 to (1) create a damage probability statistical model based on a large data set of wind

96 damage observations in the Finnish National Forest Inventory (NFI), (2) compare three

97 statistical and machine learning methods for creating the model: GLM, GAM and BRT, (3)

98 calculate a damage probability map by combining the model with national extent GIS layers

99 of model predictors, compiled from different sources, and (4) test the performance of the

100 map with independent damage observations from new NFI data.

101 2. Material and methods

102 2.1 National Forest Inventory and wind damage observations

103 In this study, we used stand level wind damage observations from the 11th Finnish national

104 forest inventory (NFI11) to create an empirical model of wind damage probability (Fig. 1).

105 The field work for the NFI11 was conducted from 2009 to 2013 (Korhonen, 2016; Korhonen

4

106   et al., 2017). In later stages of the study, we also used NFI12 (field work in 2014 to 2018) to

107   test the created map (see section 2.5).

108   In our analysis, we only included plots that were defined as forest land. Poorly productive

109   forests were excluded because they are unimportant for forestry and their wind damage risks

110   tend to be small due to low volume of growing stock. In addition, plots on treeless stands or

111   seedling stands without upper canopy layer were excluded because seedlings have very low

112   wind damage probability (8633 plots). Plots with missing data or unrealistic (erroneous)

113   values for any of the used variables were excluded (52 plots). Plots within less than 1 km

114   from the national border were also excluded, as the data set describing local wind conditions

115   (Venäläinen et al., 2017) had edge effects (214 plots). If a plot was located on the border of

116   two or more forest stands, we only used the data from the stand where the plot centre was

117   located. The final data set consisted of a total of 41 392 NFI plots.

118   Observations of stand level wind damage and an estimate of the damage time is

119   documented in the Finnish NFI (Korhonen, 2016; Tomppo et al., 2011). Here, we used only

120   the wind damage observations that had occurred no more than 5 years before the date of

121   the field visit. Since the field work of NFI11 was done in 2009 to 2013, the data can contain

122   observations from damage that has occurred between 2004 and 2013. During these years,

123   several high impact storms affected Finland, such as cyclone Dagmar (known as Tapani in

124   Finland) in December 2011 and a series of severe thunderstorms in summer 2010.

125   The severity of damage was not considered in the analysis, because the degree of damage

126   was only recorded as cumulative effect of all damage agents, and no information of wind

127   damage severity was available in cases where there were more than one damaging agent

128   present. The restriction of the analysis to only severe damage cases would also have limited

129   the number of damage observations available. Therefore, the binary damage variable

130   contains stands with different damage severities. Stand level wind damage was observed at

131   1 070 plots of the total 41 392 NFI plots in the dataset.

132

133
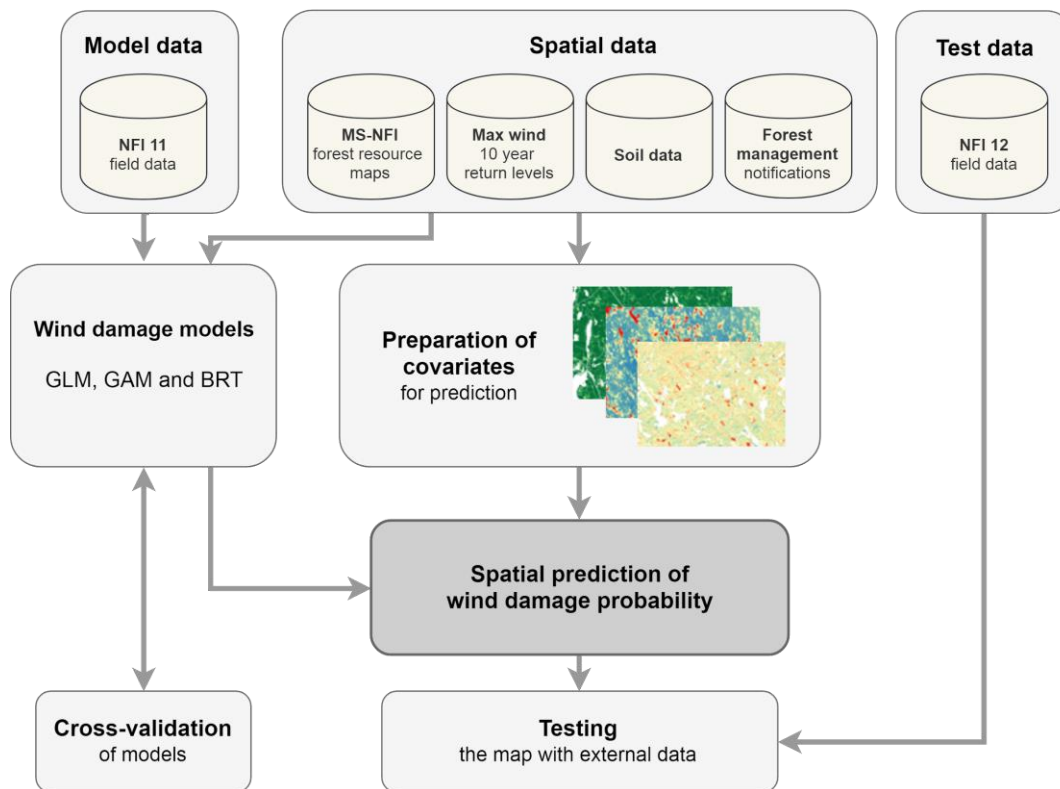
Figure 1. General approach and workflow

135

2.2 Model predictors

2.2.1 National Forest Inventory data

Most predictors in the statistical models were extracted from the NFI field data (Table 1 and 2). To describe the forest characteristics of the stand, dominant tree species and mean tree height in the stand were used. If several canopy layers and species were recorded in the data, the values from the layer with largest tree height were used, as the tallest trees can be assumed to be most vulnerable to wind. The NFI also documents the type and time of most recent forest management operation, and based on this data we created a variable describing the time since last thinning.

NFI information about soil type, soil depth and site fertility was also used (Table 1 and 2). Soil type variable differentiated between organic and mineral soils, as well as fine and coarse grained mineral soils. Fine mineral soils included clay and fine sands, whereas sands

6

148   and coarser soils were classified as coarse mineral soils. Grain size was estimated on the

149   field by NFI teams. Site fertility classes in the NFI are estimated in eight classes, but in our

150   analysis they were regrouped into two classes so that class "Fertile" contained sites from

151   herb-rich to mesic forests on mineral soils and from euthrophic to meso-oligothrophic

152   peatlands. Less fertile classes were included in the "Poor" fertility class (see Tomppo et al.,

153   2011 for detailed description of the site fertility classes used in Finnish NFI).

154   The used data covers the whole country and contains damage observations from several

155   years and several storm events. Therefore, not all plots were exposed to similar wind

156   conditions and this needed to be taken into account in the statistical model. However, we did

157   not have reliable data available about the spatial variation in maximum wind speed

158   conditions during the study period and lacking such an important factor affecting the damage

159   probability is likely to bias the estimation of the effects of other predictors. Therefore, a

160   different approach was taken. To account for areas subjected to severe storm events,

161   variable "Damage density ratio" was calculated using the locations of NFI plots as as the

162   ratio of 2D kernel density of damaged plots and all plots (Table 1). That is, the ratio

163   describes the spatial density of damaged plots in comparison to all NFI plots included in the

164   model and a value of 2, for example, can therefore be interpreted as two times higher

165   density of damaged plots than what would be expected from the density of all plots. The

166   damage density variable was then transformed into a categorical variable (with classes 0-2,

167   2-3, and >3). The upper limit of the lowest class was set relatively high to identify only the

168   strongest clusters of damaged plots and to avoid catching all the large-scale spatial trends

169   with this variable. The calculations were done in R with the *KernSmooth* package (Wand,

170   2015) using bandwidth of 20 km, see details in S1.

171   2.2.2 Other data sets and the delineation of forest stands

172   In addition to the NFI field data we also supplemented the model predictor set with additional

173   variables describing local wind conditions and open forest borders from other data sources

174   (Table 1 and 2). For the wind conditions, we used a data set describing the local 10-year

7

175   return levels of maximum wind speeds in 20 x 20 m^2 raster cells (Venäläinen et al., 2017).

176   That is, the value of each pixel represents the level of maximum wind speed (ms^{-1}) expected

177   to be reached on average once in every 10 years. The data is downscaled from coarse-scale

178   wind speed estimates in ERA-Interim reanalyzed data with a wind multiplier approach using

179   CORINE land-use data and digital elevation model (Venäläinen et al., 2017). The data set

180   contains maximum wind speeds calculated for eight different wind directions, and in this

181   study we used the maximum value of these for each pixel. To identify stands with open

182   forest borders (variable 'Open neighbour stand', Table 1), we used the multi-source NFI

183   forest resource maps (MS-NFI; Mäkisara et al., 2016; Tomppo et al., 2008) that combine

184   satellite data and NFI field data to create national extent forest resource maps in a 16 x 16

185   m^2 resolution grid.

186   However, the used wind damage observations were documented on the level of forest

187   stands and the stand borders were not mapped in the data but only estimated by the NFI

188   team at the field. Therefore, in order to combine the stand-level damage information with

189   other data sources, the locations of stand borders first needed to be defined. A forest stand

190   in the the Finnish NFI is defined as spatially continuous land area that is homogeneous with

191   respect to properties such as administrative boundaries, site fertility, structure of the growing

192   stock (e.g. maturity class, tree species composition) and forest management (Tomppo et al.,

193   2011). To create polygons that would approximately correspond to the stands assessed in

194   the field by the NFI team, we used image segmentation on the MS-NFI data layers

195   (corresponding to year 2013) describing growing stock volumes by main tree species groups

196   (pine, spruce and deciduous species) and tree height. Land property boundaries obtained

197   from the National Land Survey of Finland were also included in the segmentation, as they

198   are considered as stand boundaries in the NFI. The image segmentation was conducted

199   with the methodology described by Pekkarinen (2002), using the "segmentation by directed

200   trees" algorithm by Narendra and Goldberg (1980).

8

201   Once the stand polygons were defined with image segmentation, they were used for

202   calculating local wind conditions and finding stands with open stand borders. For each stand

203   polygon, maximum wind-speed within the stand boundaries was calculated (Table 1).

204   Maximum value was used because the NFI field data does not specify the exact location of

205   the damage within the stand, and we assumed that damage occurred in the most wind

206   exposed part of the stand.

207   To identify plots with open neighbor stands, median tree height was first calculated for each

208   stand polygon using the MS-NFI tree height data. A stand was defined to have an open

209   stand neighbor if the median tree height of any of the stand neighbours was smaller than 5

210   meters (Table 1). Median was used instead of mean so that it would be less affected by

211   possible outlier values resulting from inaccuracies in defining the stand polygons.

212   Calculations of maximum wind speeds and open stand neighbors for the segments were

213   conducted with PostGIS (version 2.4.0) and Python (version 2.7.12) with packages

214   *geopandas* (version 0.3.0) and *rasterstats* (version 0.12.0).

2.3 Statistical modelling

216   Damage probability models were created using three different methods: generalized linear

217   models (GLM), generalized additive models (GAM, Wood 2006) and boosted regression

218   trees (BRT; Elith et al., 2008). In all the models the dependent variable was the presence of

219   wind damage in the stand and independent variables described forest characteristics, forest

220   management history, soil and site type, the 10-year return level of maximum wind speed and

221   temperature sum (Table 1).

222   Binomial GLM with logit-link function were fitted in R (version 3.5.1, R Core Team, 2017). To

223   account for non-linear relationships, logarithm transformation were tested for all continuous

224   independent variables and included in the final model if they showed lower AIC than models

225   with non-transformed variables. The transformations were included only for the GLM model,

226   since GAM and BRT enable more flexibility in the shapes of the relationship between

9

227   response variable and predictors, and can therefore account for non-linear relationships

228   without transformations.

229   Variable selection was based on several criteria: (1) only variables that, based on earlier

230   research, were expected to have a causal effect to wind damage probability were included,

231   (2) since the ultimate goal of the model was to produce the damage probability map, we only

232   included variables for which reasonably high-quality national-extent GIS data sets were

233   available or could be derived from existing data, (3) the behaviour of the variable in the

234   model was plausible based on existing understanding of forest wind damage. We also aimed

235   to build the model so that all major components related to wind damage probability were

236   included. Collinearity of predictors was inspected with Pearson's correlation coefficients and

237   generalized variance inflation factors (GVIF, Fox and Monette, 1992). All correlation between

238   included continuous predictor variables were weaker than 0.5 and GVIFs for all variables

239   were lower than 4.

240   Generalized additive model (GAM) is a generalized linear model with a linear predictor

241   involving a sum of smooth functions of covariates. This specification of the model in terms of

242   smooth functions instead of detailed parametric relationships allows for more flexibility in the

243   dependence of the response of the covariates (Wood, 2017). In our analysis, GAM with logit-

244   link function was fitted in R with package *mgcv* (version 1.8-24, Wood, 2011), using the

245   same predictors that were included in the GLM. All continuous predictors were included in

246   the model through non-linear smoothing spline functions. The dimension parameter (k),

247   effectively setting the upper limit on the degrees of freedom related to the smooth, was set to

248   15 for all variables, except for temperature sum for which k=5 was chosen to avoid

249   unrealistically fluctuating large-scale patterns in the predictions. The effective degrees of

250   freedom (edf) after fitting the model were lower than k for all of the terms (see S2 for details),

251   suggesting that the chosen k's were sufficiently large.

10

252   Boosted regression trees (BRT) is an ensemble method, that combines a large number of

253   regression trees with a boosting algorithm (Elith et al., 2008). Here, BRTs were computed

254   with R package *dismo* (version 1.1-4, Hijmans et al., 2017). To find the best parameters,

255   BRTs with different parameter combinations of tree complexity (tested values 1, 2, 3 and 5),

256   learning rate (0.05, 0.01 and 0.005) and bag fraction (0.5, 0.6 and 0.75) were fitted. The

257   number of trees was not assigned manually, but was estimated with k-fold cross-validation

258   using the function *gbm.step* (Hijmans et al., 2017). To estimate the number of trees and to

259   compare different parameter combinations, *gbm.step* was run separately for each parameter

260   combination. Following the rule-of-thumb suggested by Elith et al. (2008), we excluded

261   parameter combinations that led to models with fewer than 1000 trees. Thus, the model with

262   parameter combination leading to lowest holdout residual deviance in the cross-validation

263   performed by *gbm.step* and at least 1000 trees was chosen for the final model (tree

264   complexity=2, learning rate=0.01, bag fraction = 0.5, 2250 trees, see Supplementary

265   material for details).

266   To make sure that the unbalanced ratio of damaged versus non-damaged plots did not affect

267   the results, BRTs were fitted also from two balanced datasets where the balancing of the

268   observations was done by (1) undersampling the non-damaged plots or (2) oversampling the

269   damaged plots. In both cases the cross-validated AUCs were very similar to ones calculated

270   from the original unbalanced dataset and, therefore, the original data set was used for the

271   final results.

272   To account for the sampling design, weights based on the forest area each plot represents

273   were used in all models (Korhonen, 2016). For example, in northern Finland the NFI

274   sampling design is sparser and therefore the weight of one plot in modelling is higher. To

275   test if the clustered sampling design had an effect on the results, GLMs and GAMs were also

276   fitted as mixed models (GLMM and GAMM) with plot clusters as random intercepts, using R

277   packages lme4 (Bates et al., 2015) for GLMM and gamm4 (Wood and Scheipl, 2017) for

278   GAMM. However, as the mixed model predictions (in the scale of the linear predictor, using

11

279   only fixed effects for prediction) were highly correlated with the fixed effect model prediction

280   (Pearson's r=0.998, p<0.001 for GLM vs GLMM, and r=0.979, p<0.001 for GAM vs GAMM)

281   and our interest was in marginal instead of conditional inference, no random effects were

282   included in the final models.

283   The models were validated with 10-fold stratified cross-validation, where number of

284   damaged plots was divided evenly into the folds. In the cross-validation, the variation in

285   damage density variable was not used in the prediction, because the variable was included

286   in the model only to account for spatial structures in storm severity in the data, and in an

287   aimed use case of the models (i.e., estimating damage vulnerability in future events) we

288   would not have this information available. Instead, separate predictions for test-folds were

289   calculated with each class of the damage density variable (0-2, 2-3, >3). Then, these three

290   predictions were averaged based on the frequency of each class in the original model data.

291   See details in S1.

292   ROC curves and AUC values were calculated for each iteration of cross-validation and used

293   to assess the performance of the models (see Supplementary material). The ROC curve

294   plots the true positive rate (sensitivity) and true negative rate (specificity) of the model with

295   all possible classification thresholds. The AUC values represent the area under ROC curve

296   and measure the model's ability to discriminate between events and non-events. AUC

297   values of 0.5 corresponds to a situation where the classifier is no better than random (ROC

298   curve along diagonal) and value of 1 a situation where the model perfectly discriminates

299   between events and non-events. As a rule of thumb, AUC values over 0.7 are considered

300   acceptable discrimination between classes, values over 0.8 excellent and values over 0.9

301   outstanding (Hosmer et al., 2013).

302

12

303 **Table 1.** Description of predictors used and their sources in the model and in the damage
304 probability map. See section 2.2.1 for details.

Variable	Type*	Unit / Classes	Source in model	Source in map
Tree species	C	pine, spruce, other	NFI11	MS-NFI 2015
Tree height	N	dm	NFI11	MS-NFI 2015
Time since thinning	C	0-5, 6-10, > 10 years	NFI11	MS-NFI 2015, Forest use notifications
Wind (10-year return level of max wind speed)	N	ms^{-1}	Venäläinen et al. 2017	Venäläinen et al. 2017
Open neighbor stand	C	True, False	MS-NFI 2013	MS-NFI 2015
Soil type	C	Mineral/coarse, Mineral/fine, Organic	NFI11	GTK 2018, NLS 2018
Mineral soil depth < 30 cm	C	True, False	NFI11	GTK 2018, NLS 2018
Site fertility	C	Fertile, Poor	NFI11	MS-NFI 2015
Temperature sum (average 1985-2014)	N	100 dd (over 5C)	Aalto et al. 2016	Aalto et al. 2016
Damage density ratio	C	0-2, 2-3, <3	NFI11	In the calculation of the map, this variable was included as a weighted average of all classes, because it was included in the model only to account for spatial structures in storm severity.

305 *C – categorical, N – numerical (continuous)*
306

307

13

308 **Table 2.** Descriptive statistics for the NFI11 data. Mean and standard deviation for non-
309 damaged, damaged and all plots continuous variables, and percentages of each class for
310 categorical variables. The definitions of the variables are in table 1.

	Non-damaged	Damaged	All
Number of plots	40322	1070	41392
Species			
Scots pine	63.4%	59.1%	63.3%
Norway spruce	24.0%	36.8%	24.3%
Other	12.6%	4.1%	12.4%
Tree height	163.0 (50.5)	195.2 (45.1)	163.9 (50.6)
Time since thinning			
0-5 years	13.4%	26.0%	13.7%
6-10 years	9.2%	15.5%	9.4%
> 10 years	77.4%	58.5%	76.9%
Wind	12.1 (2.0)	12.5 (2.0)	12.2 (2.0)
Open neighbor			
False	85.7%	84.6%	85.7%
True	14.3%	15.4%	14.3%
Soil type			
Mineral, coarse	66.9%	77.8%	67.2%
Mineral, fine	12.7%	9.8%	12.7%
Organic	20.3%	12.4%	20.1%
Soil depth < 30 cm			
False	89.5%	85.0%	89.4%
True	10.5%	15.0%	10.6%
Site fertility			
Poor	34.8%	31.9%	34.7%
Fertile	65.2%	68.1%	65.3%
Temperature sum	1185 (178.9)	1262.6 (130.4)	1187.0 (178.3)

311

14

2.4 Calculation of the damage probability map

A GIS raster data layer with resolution of 16 x 16 m^2 and extent of the whole country was prepared for each predictor variable used in the models (Table 1). Forest variables (dominant species, tree height, height-diameter ratio, open forest edge) were derived from the most recent Finnish MS-NFI data for year 2015 (Mäkisara et al., 2019). A grid cell was defined to be on an open forest edge if tree height in the MS-NFI data was lower than 5 meters in any of the cell's within a 5 x 5 cell neighborhood.

Spatial data on forest management history (the time of last thinning) was derived from the forest use notification collected by the Finnish Forest Centre. This data consists of forest use notifications that forest owners are required to report to the Forest Centre before conducting management operations in their forests. For each 16 x 16 m^2 pixel, we first assigned the year of the latest notification of planned thinning in that location of the pixel and then calculated the difference to year 2015.

Data for the 10-year return rates of maximum wind (Venäläinen et al., 2017) was resampled to the 16 x 16 m^2 grid with GDAL using bilinear interpolation. Soil type was defined as ORGANIC for areas within the peatland polygons in the Topographic Database produced by the National Land Survey of Finland (NLS, 2018). Other areas were defined as mineral soils, and further divided to fine or coarse mineral soils based on the top soil information in the 1:200 000 resolution soil map of the Geological Survey of Finland (GTK, 2018). Data layer for soil fertility classes was made by reclassifying the MS-NFI fertility class data layer from the original five classes to the two classes used in the models (see details in section 2.2.1). Average annual temperature sum was calculated with a threshold of 5°C from daily weather data grids (Aalto et al., 2016) for the years 1985 to 2014.

Similarly as in the cross-validation, the variation in damage density variable was not used in the prediction, because we would not have this information available for future events. Instead, separate predictions were calculated with each class of the damage density variable

15

338   and these three predictions were then averaged based on the frequency of each class in the

339   original model data. See details in S1.

340   The damage probability map was calculated from the GLM, GAM and BRT model objects

341   and the GIS data layers using R packages *raster* (Hijmans, 2017) and *sp* (Pebesma and

342   Bivand, 2005).

2.5 Testing the map with new damage observations

344   The accuracy of the damage probability map was validated with an independent test data

345   set. The map was compared to the damage observations in the most recent NFI

346   measurements (12th Finnish NFI, NFI12), which were not included in the model fitting data

347   that was from the NFI11. Compared to NFI11, which covers the whole country, NFI12 does

348   not cover the northernmost parts of Finland as plots in the three most northern municipalities

349   (Northern Lapland), where the proportion of forest land is low, are not measured as

350   frequently as other parts of the country.

351   We included the NFI12 plots that had been measured during 2014-2018, were classified as

352   forest land by the field team, and were located within forest area in the MS-NFI forest

353   resource maps (i.e., there were data in the wind damage probability map at the location of

354   the plot). For wind damage we also used the same criteria as with the model data, i.e. only

355   observations estimated to have occurred during the last 5 years were included and the

356   severity of the damage was not considered. In addition, those permanent plots that were

357   measured already in NFI11 were excluded from the test data, as the previous

358   measurements in the same plots were used in the model fitting. The final test data consisted

359   of 33 754 plots with wind damage in 734 of the plots.

360   Values of the wind damage probability maps were extracted at the locations of test data

361   plots as the mean value of map pixels within 20 meter buffer from the location of the plot

362   center. ROC curves and AUC values were calculated from the wind damage information in

363   the test data and the extracted values of the damage probability maps. The extraction was

16

364   conducted in R with package *raster* (version 2.8-19, Hijmans, 2017) and ROC/AUC

365   calculations with package *pROC* (version 1.12.1, Robin et al., 2011).

3. Results

367   The results showed that forest vulnerability to wind damage is strongly driven by forest

368   characteristics, especially tree height (Figs 2-4, Table 3). In all models, the damage

369   probability increased with tree height, and the increase was strongest for spruce dominated

370   forests. Also forest management affected damage probability in the models, as recently

371   thinned forests and forests with open stand borders were more susceptible to damage.

372   These predictors, related to the forest characteristics, very much drive the fine-scale spatial

373   variation of damage probability in the (Fig. 7).

374   Wind damage probability was found to show distinct large-scale trends, most importantly the

375   decreasing damage probability from south to north (Fig. 7). This effect in the models comes

376   from the temperature sum, but also other predictors contributed to the large-scale trends in

377   the map, as there as large-scale patterns in wind conditions, forest characteristics and soil

378   and site fertility conditions (Figs 2-4). The north-south pattern in damage density was evident

379   in the damage probability maps with all model methods. However, the map created with the

380   BRT model showed unexpectedly high damage probability values for the northernmost parts

381   of the country (Fig. 7).

382   The model predictors showed in general rather similar effects in the three tested methods

383   (GLM, GAM and BRT). Yet, there are also differences, especially in the shape of relationship

384   between the continuous predictors and predicted damage probability (Figs 2-4). In GLM, the

385   relationships are restricted to sigmoidal curves, whereas GAM and BRT allow more flexible

386   shapes of responses. This can be seen, for example, in how increasing tree height in pine

387   forests shows steadily increasing damage probability with GLM (Fig. 2) whereas in GAM

388   damage probability peaks around tree height 200 dm and then declines. Higher values of

389   damage density ratio led to higher damage probability in all models, as expected (Fig. 5).

17

390   As the BRT predictions are calculated from ensembles of regression trees, they enable very

391   sharp changes in the prediction within small changes in the predictor (Fig. 4). They can also

392   contain diverse interactions between the predictors, which are unfortunately not visible in

393   partial dependence plots like Fig. 4. The BRT results showed somewhat different trends than

394   the other methods in model responses to predictors (Fig. 4). For example, while tree height

395   in spruce forests increases damage probability throughout the range of data in GLM and

396   GAM results (Figs 2-3), in BRT results similar strongly increasing trend is not found, instead

397   the relationship between height and damage probability seems to saturate for all tree

398   species (Fig. 4). The large-scale spatial patterns in map prediction also differed for BRT

399   compared to the other models, as high values of damage probability were predicted for the

400   northernmost parts of the country. (Fig. 7).

401   Cross-validation showed higher predictive performance of the GAM model compared to the

402   GLM and BRT (Fig. 6). However, when the final damage probability maps were tested with

403   the NFI12 test data, all models showed very similar performance in discriminating between

404   damaged and non-damaged plots in the test data. (Fig. 8). All maps gave on average higher

405   damage probability values for damaged than non-damaged plots and showed an acceptable

406   level of discrimination between the two (AUC > 0.7). The added flexibility and ability to

407   account for nonlinear relationships in GAM and BRT did not considerably improve the

408   predictive performance of maps compared to the fully parametric GLM (Fig. 8).

409

410

18

411 **Table 3.** GLM model results (for categorical variables, the first class listed in Table 1 is the
412 reference class, and therefore not listed separately in this table).

	Estimate	Std. Error	z value	Pr(>|z|)
(Intercept)	-14.690	1.061	-13.841	< 0.001
Species/Spruce	-8.494	1.918	-4.430	< 0.001
Species/Other	-9.314	3.931	-2.370	0.018
log(Height)	1.661	0.189	8.807	< 0.001
Last thinning/6-10 years	-0.298	0.113	-2.637	0.008
Last thinning/over 10 years	-0.844	0.084	-9.995	< 0.001
log(Wind)	0.749	0.238	3.152	0.002
Open stand border / TRUE	0.310	0.095	3.284	0.001
Soil/mineral, fine	-0.356	0.124	-2.875	0.004
Soil/organic	-0.216	0.110	-1.962	0.050
Soil depth < 30cm / TRUE	0.214	0.106	2.011	0.044
Site fertility / Fertile	-0.425	0.092	-4.611	< 0.001
Temperature sum	0.096	0.025	3.843	< 0.001
Damage density / 2-3	1.104	0.088	12.498	< 0.001
Damage density / >3	1.898	0.111	17.137	< 0.001
Species/Spruce : log(Height)	1.634	0.358	4.561	< 0.001
Species/Other : log(Height)	1.625	0.742	2.190	0.029

413

414

19

415

416
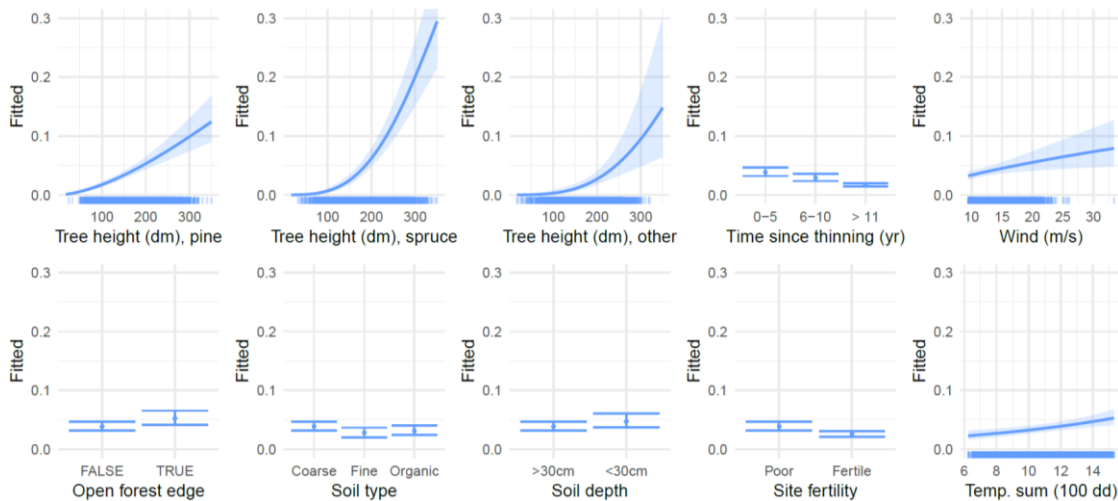
Figure 2. GLM partial dependence plots for the map predictors. Prediction of damage probability is calculated for the range of each predictor variable when other predictors are set to average (continuous variables) or reference class (categorical variables). Rugged x-axis describes the distribution of data. Confidence intervals are calculated as 2 x prediction standard error (in the scale of the linear predictor).

422

423

424
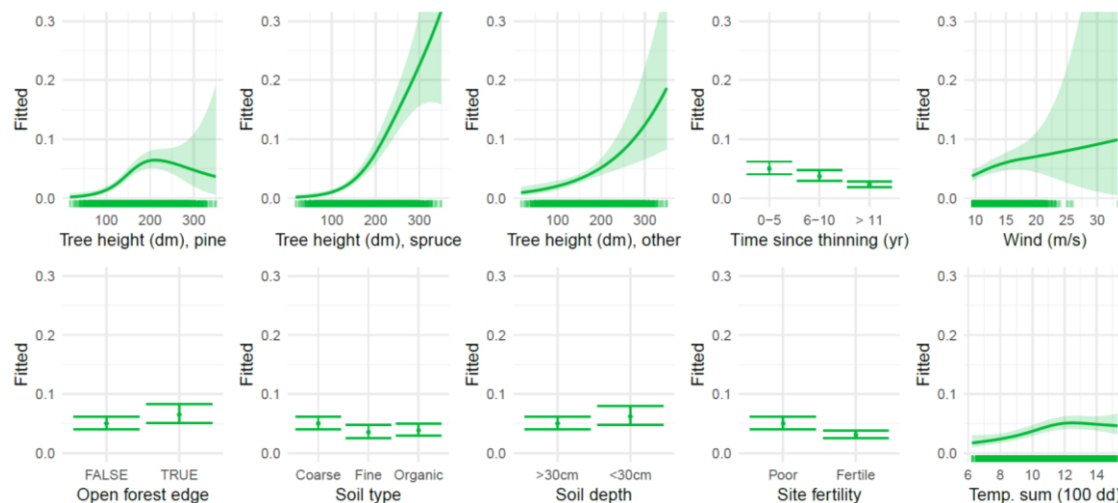
Figure 3. GAM partial dependence plots for the map predictors. Prediction of damage probability is calculated for the range of each predictor variable when other predictors are set to average (continuous variables) or reference class (categorical variables). Rugged x-axis describes the distribution of data. Confidence intervals are calculated as 2 x prediction standard error (in the scale of the linear predictor).

20
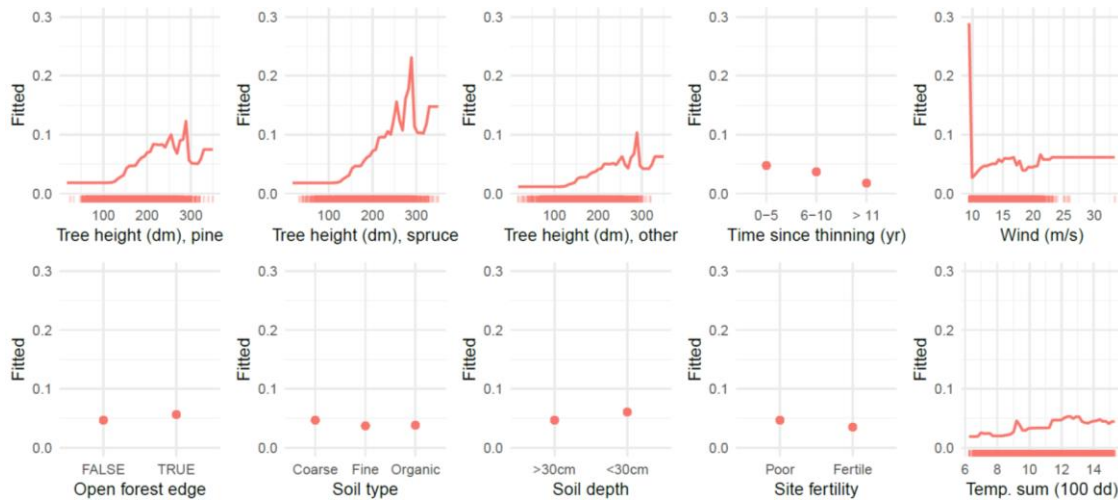
Figure 4. BRT partial dependence plots for the map predictors. Prediction of damage probability is calculated for the range of each predictor variable when other predictors are set to average (continuous variables) or reference class (categorical variables). Rugged x-axis describes the distribution of data.
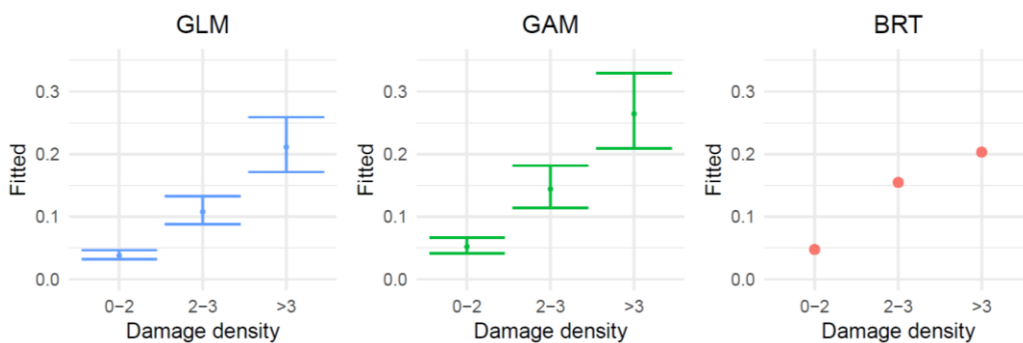
Figure 5. Partial dependence plots for damage density in the different models (GLM, GAM and BRT). Damage density was included in the models to account for spatial variation in severity of storm damage in the data, and it was set to 0 when calculating the wind damage probability map. Note that the y-axis range differs from figures 2-4.

21

443
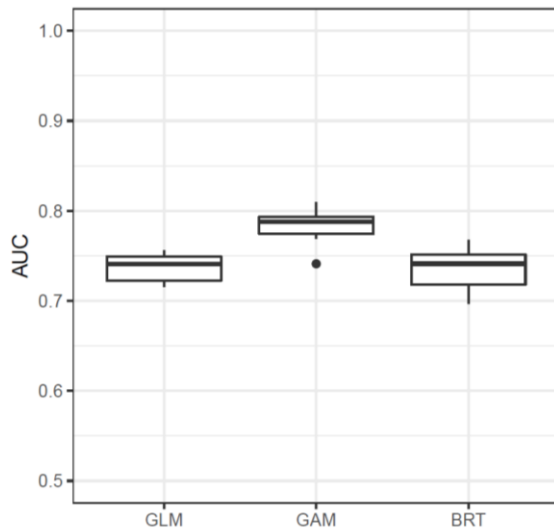
Figure 6. Distribution of AUC values in the 10-fold cross-validation for GLM, GAM and BRT.

445

446
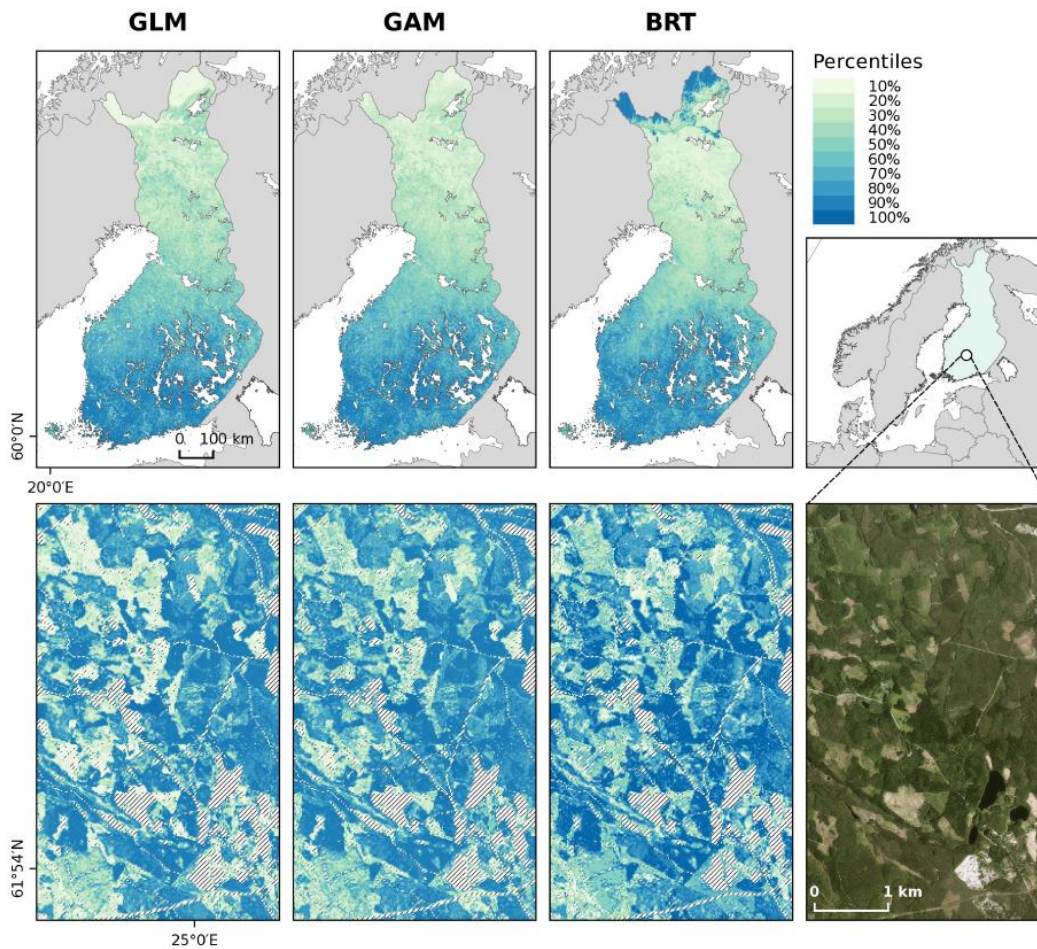
Figure 7. Damage vulnerability maps calculated for the whole country (upper panel) and a fine-scale detail of the maps (lower panel), calculated with the three different damage probability models (GLM, GAM and BRT), and an orthophoto from the same location (B). Colors in the damage vulnerability map are defined by the percentiles of the map data (e.g., the first class contain the lowest 10% of map values). The upper panel maps are resampled

22

452 to 1 km x 1 km resolution with bilinear interpolation. Note that the orthophoto is not from the

453 exact same time as the forest resource data used for the calculation of the map. Orthophoto

454 © National Land Survey of Finland.

455

456

457
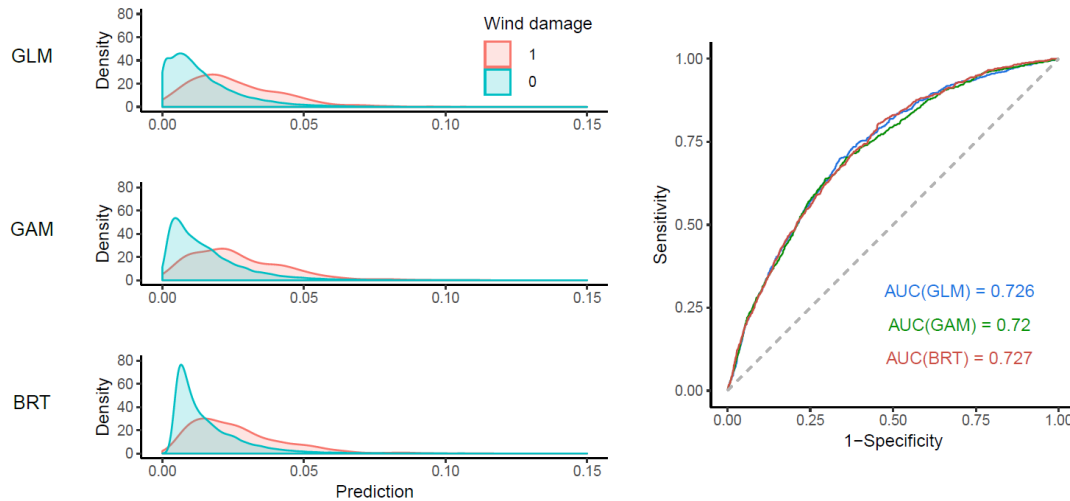
Figure 8. Density plots of the distributions of map predictions for test data plots with wind
damage (red) and without wind damage (blue), and ROC curve showing the ability of the
maps to distinguish between damaged and non-damaged test plots for the different model
methods (GLM, GAM and BRT).

462

4. Discussion

4.1 The damage probability map

We created a new spatial wind damage risk product based on inventory data spanning over

several years and several other data spatial sources, including information where the actual

harvests have recently occurred in Finland. Validation of the map with independent and large

data dataset showed that the map is able to identify vulnerable stands also in new storm

events. While there have been attempts to map wind damage probability based on empirical

damage models (Saarinen et al., 2016; Schindler et al., 2009; Suvanto et al., 2016), our

work here uniquely provides national extent and high spatial resolution information about

forest vulnerability to wind and is also tested with large external test data.

23

473   The successful identification of damage vulnerability in the independent test data is not

474   trivial. First of all, wind damage is challenging to predict and extending the performance of

475   statistical wind damage models to new data sets has been shown not to be straightforward

476   (Fridman and Valinger, 1998; Kamimura et al., 2015; Lanquaye-Opoku and Mitchell, 2005).

477   Moreover, because we wanted to test how well our map identifies forest vulnerability to wind

478   in future events, for which we don't have detailed information of, we did not include any

479   information about spatial distribution of wind speeds or storm events during the time frame of

480   the test data when we tested the map. Thus, the discrimination of damaged from non-

481   damaged plots with fair accuracy (AUC=0.72) for the entire extent of Finland indicates that

482   the map is indeed successful in identifying the vulnerable forests, and implies that efficient

483   combination of inventory data and several new spatial data sources is a promising way to

484   map damage risks.

485   A major factor contributing to the successful extension of the map to new test data was the

486   large and systematically sampled forest and damage data that spanned over several years.

487   Thus, our model was able to represent the different conditions (forest characteristics, soil,

488   etc.) within the country. The need for comprehensive model data in empirical wind damage

489   models has been demonstrated, for example, by Hart et al. (2019) who showed that it is

490   possible to generalize to new storm events when the model data covers the variation of

491   predictor variables in the new data set.

492   In addition to good representation of environmental and forest conditions, our data also

493   represents different types of wind events, since the data consisted of damage observations

494   in a 5-year time window. Most wind disturbance studies typically concentrate on one or few

495   storms (e.g., Hart et al., 2019; Kamimura et al., 2015; Saarinen et al., 2016; Schindler et al.,

496   2009; Suvanto et al., 2016), which limits their ability to generalize to different storm events.

497   While modelling of multi-event data can be more challenging than single-event data

498   (Albrecht et al., 2019), we argue that it is necessary when the purpose of the model is in

499   assessing damage probability in future events.

24

500 Availability of high-quality and high-resolution spatial data of the model predictors was also

501 crucial in the successful creation of the damage probability map. Additional uncertainties

502 arise from the input data sets when model predictions are made with GIS data gathered from

503 several different sources instead of the field-measured data that were used for fitting the

504 model. In our case, we were able to utilize several high-quality and high-resolution data

505 sources, such as the MS-NFI raster maps of forest characteristics (Mäkisara et al., 2019)

506 and new data products of local wind conditions (Venäläinen et al., 2017). We were also able

507 to use the recently opened forest use notification data from the Finnish Forest Centre that

508 provided us with nation-wide information about the recent forest management history of the

509 stands. This type of legacy information about forest management is typically difficult to

510 obtain and has rarely been included in predictive wind damage risk models before, despite

511 the clear effects of management history on forest disturbance dynamics. While all these data

512 sources contain uncertainties, the verification of our map with independent test data showed

513 that they were nevertheless able to represent well the main factors determining forest

514 susceptibility to wind.

515 With new data sources and increasing quality and availability of data in the future, the

516 accuracy of the map could still be improved. This could mean, for example, improved

517 accuracy of tree height information through the use of lidar data or inclusion of variables that

518 were left out of the current map due to lack of national level spatial data about their

519 distribution (e.g. distribution of wood decaying fungi that weaken trees' resistance to wind).

520 Soil data had maybe the lowest resolution and higher uncertainties of the used GIS data

521 and, therefore, increased quality of those data sets would also be desirable. However, the

522 effects of soil variables in the model were relatively small, and therefore the effects of only

523 improving the soil GIS data in the prediction would most likely not be drastic. Instead, more

524 detailed soil data would be needed for the model data to improve the description of the role

525 of soil characteristics on tree vulnerability to wind in the model.

25

4.2 Drivers of forest susceptibility to wind disturbance

The factors that were found to affect damage probability in our results are well in line with previously published results. For example, increasing damage probability with tree height and the higher vulnerability of Norway spruce have been shown in previous studies (Peltola et al., 1999; Suvanto et al., 2016; Valinger and Fridman, 2011). New stand edges after clearcutting of the neighboring stand and recently thinned stands have also been known to be at higher risk of windthrow (Lohmander and Helles, 1987; Peltola et al., 1999; Wallentin and Nilsson, 2014).

While open stand edges did increase the risk of wind damage in our results, the effect was not as distinct as could be expected from earlier research that emphasizes the role of forest edges (e.g., Peltola et al., 1999). This may in part result from the use of stand level data, where defining and identifying the open stand borders from the NFI data is more uncertain than in the case of tree-level analysis (see section 2.3.2 for the used methodology). Earlier work with storm damage data from severe autumn storms in Finland showed that the effects of open forest edges on damage probability were more emphasized in tree-level analysis (Suvanto et al., 2018) than in the stand-level analysis of the same data (Suvanto et al., 2016). In the future, potential improvements to the presentation of damage probability at the forest edges in the map could be achieved by combining tree-level results or mechanistic approaches to the current stand-level modeling approach.

In the model, the effect of wind speed data (Venäläinen et al., 2017) on damage probability showed logical behaviour of increasing damage probability with increasing 10-year return rates of maximum wind speed. The wind speed data accounts for the effects of topography on general wind conditions, and therefore variables describing topographical conditions were not included in our models, even though they have been shown to be linked with wind damage probability (e.g., Schindler et al., 2009).

26

551   Large-scale geographical patterns in our results showed that the probability of wind damage

552   in Finland decreases from south to north. This is in agreement with results form previous

553   studies combining forest model simulations with mechanistic wind damage models (Ikonen

554   et al., 2017; Peltola et al., 2010). The higher susceptibility of forests in southern Finland to

555   wind disturbances is related to the shorter length of the soil frost period in southern parts of

556   the country. When the soil is frozen, trees are well anchored to the ground and less

557   vulnerable to windthrow and, therefore, forests located in areas with longer periods of soil

558   frost are less likely to be damaged during winter storms (Gregow et al., 2011; Laapas et al.,

559   2019) (Gregow et al., 2011). However, other factors affecting forest wind susceptibility also

560   change along the north-south gradient. The proportion of Scots pine, a species more

561   resistant to wind than Norway spruce, increases towards north, and trees in the north have

562   on average lower height-to-diameter ratio, which is linked to wind damage sensitivity (Ikonen

563   et al., 2017; Peltola et al., 2010). In addition, in southern parts of the country, forest stands

564   are smaller in area and there are less protected areas compared to the north. Thus, more

565   frequent windthrows related to new stand edges and recent thinnings may also contribute to

566   higher damage probability in the south. Similarly, butt rot caused by *Heterobasidion* sp.,

567   which increases tree vulnerability to wind (Honkaniemi et al., 2017), currently affects the

568   southern parts of the country more severely (Mattila and Nuutinen, 2007; Müller et al., 2018)

569   and may also contribute to the north-south pattern in the wind damage probability in our

570   results. Therefore, it is not entirely clear what are the exact mechanisms causing increased

571   damage probability with temperature sum in our model.

572   ## 4.3 Comparison of methods

573   While the results for GLM and GAM models were rather similar, the BRT showed rather

574   different model behaviour and large scale prediction patterns. The lack of test data in the

575   northernmost parts of the country makes the interpretation of the test results (Fig. 8) for the

576   BRT a bit challenging, as the area with unexpected BRT predictions is mainly not covered by

27

577   the test data. In any case, the high values of BRT predictions in northernmost Finland do not

578   seem realistic.

579   Our results did not show improved predictive performance of the map with the more flexible

580   methods GAM and BRT compared to the logistic regression model (GLM). This is somewhat

581   surprising, especially in the case of BRTs, because several recent studies have shown good

582   performance of random forest for modelling storm disturbances (Albrecht et al., 2019; Hart et

583   al., 2019; Kabir et al., 2018). Yet, in our results BRT did not lead to better predictive

584   performance in cross-validation or with test data, even though it is a tree-based ensemble

585   method very similar to random forest.

586   Our analysis differs from that of these earlier studies (Albrecht et al., 2019; Hart et al., 2019;

587   Kabir et al., 2018) on a few aspects. First, we modelled wind damage on the level of forest

588   stands, whereas the above mentioned studies were operating on tree-level. Second, we

589   were using longer term NFI damage observations whereas most others used data from

590   specific storm events. However, the study by Albrecht et al. (2019) contained both event-

591   specific and non-event-specific data and they found random forests to outperform GLMs in

592   both types of data. Third, we performed the cross-validation without considering the spatial

593   variation in the storm conditions (the damage density variable in our analysis). This was

594   done because we did not want to use this variable in the prediction, as the final aim was to

595   generalize the results to future damage events, where this information would not be

596   available. It is possible that this approach is disadvantageous to the BRT. All these

597   differences in the approaches and analysis may have contributed in different performance of

598   methods between the studies.

599   On the other hand, while the above mentioned studies did find machine learning methods

600   outperform traditional statistical models in many ways, they also showed some positive sides

601   of the logistic models. Most importantly, even though random forests showed superior

602   performance when cross-validating models with data from one storm event in Hart et al.

28

603 (2019), logistic models showed the highest AUC values compared to the other methods

604 when the model was applied to another storm event, supporting the value of GLMs when

605 generalizing the results to new storm events.

606 It seems that while machine learning methods such as BRT and random forest have

607 advantages in accounting for more complex relationships and interactions in the data, they

608 also catch patterns that are not helpful in estimating future disturbance probabilities (see,

609 e.g., the unrealisticly high probabilities of damage with very low wind speeds in BRT, Fig. 4).

610 This is likely to hamper the performance of BRTs so that they are not able to improve cross-

611 validation performance compared to GLM.

612 Use of GLMs has the extra benefit of being more easily communicated to the end user, and

613 they can be easily applied to new use cases when model coefficient estimates are

614 published. The interpretation of relationships between predictors and the response variable

615 is more straightforward, whereas especially in BRTs very small changes in e.g. tree height

616 can lead to drastic changes in model prediction (Fig. 4). The unexpectedly high damage

617 probability values in northern Finland also demonstrate the unpredictability of BRT model

618 behaviour. This aspect is particularly important when the end product is meant to be used in

619 practical applications.

620 ## 4.4 Applications and use of the maps

621 The strength of the map is in its high resolution and large extent. The high-resolution makes

622 it useful for assessing wind damage susceptibility of individual forest stands in fragmented

623 forest landscapes where spatial variation of forest characteristics is high. On the other hand,

624 the national extent of the map makes it widely available and accessible to everyone who is

625 making forest management decisions in Finnish forests. To further improve the accessibility

626 and usability of the map, we created an openly available web map application, where users

627 can explore the map and find the estimated wind damage vulnerabilities of the forests they

628 are   interested   in,   without   expert   knowledge   in   GIS   software   (see

29

629 https://metsainfo.luke.fi/en/tuulituhoriskikartta, currently only in Finnish, click "Tuulituhoriskit"

630 box to see the wind damage vulnerability map). By providing an effective tool for identifying

631 the vulnerable stands and for communicating wind damage risks to forest managers and

632 owners, the map has potential to steer forest management practices towards a more

633 disturbance-aware direction.

634 In addition to forest management, high-resolution information about forest wind vulnerability

635 is crucially needed also in other sectors and applications. For example, the map can help in

636 identifying high-risk locations where windthrown trees can harm infrastructure by damaging

637 power lines and blocking roads. Insurance companies may also use high-resolution

638 vulnerability information for a more risk based pricing of forest insurances.

639 While wind disturbances have major consequences from the human point of view, they are a

640 natural process and have an important role in shaping the structure and function of forest

641 ecosystems (Bouget and Duelli, 2004; Kuuluvainen, 2002). By exploring the drivers and

642 spatial variability of wind disturbance dynamics, our results can therefore provide insight in

643 current disturbance regime and its effects in the ecosystem, such as biodiversity and carbon

644 cycling. Improved information about forest disturbances and tree mortality is also urgently

645 needed for vegetation models from stand to global scales to understand how forests will

646 react to the changing climate (Bugmann et al., 2019; Friend et al., 2014).

647 When applying the map in practice, it is important to consider its limitations. First, the

648 damage probabilities in the map are in reference to the damage happened during the study

649 period. The amount of wind damage varies strongly between years and future conditions are

650 not likely to exactly match the conditions during the period from which the data comes from.

651 Therefore, instead of exact probability values, it is better to interpret the map values as

652 relative differences in damage vulnerability. Second, it is important to note that the damage

653 probabilities do not only refer to complete damage of the stand, as our analysis also included

654 less severe damage cases and we did not account for damage severity. Third, it is good to

30

655   keep in mind that the map presents forest vulnerability to wind and it is not possible to

656   predict the exact location of future wind disturbances, as there are many things - such as

657   tracks and meteorological conditions of future storms - that can't be accounted for in the

658   map. The uncertainties need to be taken into consideration when using the map.

659   Wind disturbances are strongly linked to other processes of the forest and, therefore, should

660   be considered in larger context. Thus, the greatest benefits of our results can perhaps be

661   achieved by combining it with information and understanding of other processes that control

662   forest ecosystems and forest management decisions. For example, the risk model can be

663   coupled with forest growth simulators and thereafter storm damage risks of different forest

664   management strategies can be evaluated simultaneously when making future scenarios of

665   forests. The map can be combined with spatial information of wood volumes and prices to

666   assess economic risks wind disturbances. Combining wind disturbance results with the

667   dynamics of other disturbance agents is also crucial, as wind damage is strongly linked to

668   bark beetle outbreaks and root rot, and these interactions are becoming increasingly

669   important with the changing climate (Seidl et al., 2017; Seidl and Rammer, 2017). A

670   comprehensive approach is therefore needed to understand and effectively manage wind

671   disturbances in forests.

672   5. Conclusions

673   In this study, we show how probability models based on NFI damage observations combined

674   with existing spatial datasets can be used to provide a fine-scale large-extent map of wind

675   disturbance probability. We also demonstrate the ability of the map to identify vulnerable

676   stands in future events with an extensive external test data. These maps provide a powerful

677   tool for supporting disturbance-aware management decisions, communicating disturbance

678   risks to forest owners, and accounting for the effects of windthrown trees in other sectors,

679   such as maintenance of powerline infrastructures.

680   Our results show that machine learning methods, such as BRT, do not always provide

681   superior results compared to traditional statistical models. As their interpretation in also less

682   straightforward, they can sometimes lead to unpredictable prediction outcomes. Therefore, it

683   is crucial to always assess the benefits of different approaches and to carefully test the

684   performance of the used method with test data that is not used in model fitting. Partial

685   dependence plots and other ways for exploration of model predictions in different situations

686   also provide useful tools for assessing if model behaviour is realistic and biologically

687   plausible.

688   The success of our results is based on large and representative model data as well as high-

689   quality and high-resolution GIS data used as map inputs. In Finland, good data sets for both

690   the model fitting and the map inputs are available, which enabled work done in this study.

691   However, with improving data quality and availability (for both damage observations for

692   model fitting and GIS data for map inputs), similar work could be extended to other regions

693   and even to other disturbance types.

694   ## Acknowledgements

32

References

Aalto, J., Pirinen, P., Jylhä, K., 2016. New gridded daily climatology of Finland: Permutation-based uncertainty estimates and temporal trends in climate. J. Geophys. Res. Atmospheres 121, 3807–3823. https://doi.org/10.1002/2015JD024651

Albrecht, A.T., Jung, C., Schindler, D., 2019. Improving empirical storm damage models by coupling with high-resolution gust speed data. Agric. For. Meteorol. 268, 23–31. https://doi.org/10.1016/j.agrformet.2018.12.017

Andersson, E., Keskitalo, E.C.H., Bergstén, S., 2018. In the eye of the storm: adaptation logics of forest owners in management and planning in Swedish areas. Scand. J. For. Res. 33, 800–808. https://doi.org/10.1080/02827581.2018.1494305

Bates, D., Mächler, M., Bolker, B., Walker, S., 2015. Fitting Linear Mixed-Effects Models Using lme4. J. Stat. Softw. 67, 1–48. https://doi.org/10.18637/jss.v067.i01

Bouget, C., Duelli, P., 2004. The effects of windthrow on forest insect communities: a literature review. Biol. Conserv. 118, 281–299. https://doi.org/10.1016/j.biocon.2003.09.009

Bugmann, H., Seidl, R., Hartig, F., Bohn, F., Brůna, J., Cailleret, M., François, L., Heinke, J., Henrot, A.-J., Hickler, T., Hülsmann, L., Huth, A., Jacquemin, I., Kollas, C., Lasch-Born, P., Lexer, M.J., Merganič, J., Merganičová, K., Mette, T., Miranda, B.R., Nadal-Sala, D., Rammer, W., Rammig, A., Reineking, B., Roedig, E., Sabaté, S., Steinkamp, J., Suckow, F., Vacchiano, G., Wild, J., Xu, C., Reyer, C.P.O., 2019. Tree mortality submodels drive simulated long-term forest dynamics: assessing 15 models from the stand to global scale. Ecosphere 10, e02616. https://doi.org/10.1002/ecs2.2616

Dobbertin, M., 2002. Influence of stand structure and site factors on wind damage comparing the storms Vivian and Lothar. For. Snow Landsc. Res. 77, 187–205.

Elith, J., Leathwick, J.R., Hastie, T., 2008. A working guide to boosted regression trees. J. Anim. Ecol. 77, 802–813. https://doi.org/10.1111/j.1365-2656.2008.01390.x

33

731   Fox, J., Monette, G., 1992. Generalized Collinearity Diagnostics. J. Am. Stat. Assoc. 87,

732   178–183. https://doi.org/10.1080/01621459.1992.10475190

733   Fridman, J., Valinger, E., 1998. Modelling probability of snow and wind damage using tree,

734   stand, and site characteristics from Pinus sylvestris sample plots. Scand. J. For. Res.

735   13, 348–356. https://doi.org/10.1080/02827589809382994

736   Friend, A.D., Lucht, W., Rademacher, T.T., Keribin, R., Betts, R., Cadule, P., Ciais, P., Clark,

737   D.B., Dankers, R., Falloon, P.D., Ito, A., Kahana, R., Kleidon, A., Lomas, M.R.,

738   Nishina, K., Ostberg, S., Pavlick, R., Peylin, P., Schaphoff, S., Vuichard, N.,

739   Warszawski, L., Wiltshire, A., Woodward, F.I., 2014. Carbon residence time

740   dominates uncertainty in terrestrial vegetation responses to future climate and

741   atmospheric CO2. Proc. Natl. Acad. Sci. 111, 3280–3285.

742   https://doi.org/10.1073/pnas.1222477110

743   Gregow, H., Laaksonen, A., Alper, M.E., 2017. Increasing large scale windstorm damage in

744   Western, Central and Northern European forests, 1951–2010. Sci. Rep. 7, 46397.

745   https://doi.org/10.1038/srep46397

746   Gregow, H., Peltola, H., Laapas, M., Saku, S., Venäläinen, A., 2011. Combined occurrence

747   of wind, snow loading and soil frost with implications for risks to forestry in Finland

748   under the current and changing climatic conditions. Silva Fenn. 45.

749   https://doi.org/10.14214/sf.30

750   GTK, 2018. Superficial deposits of Finland 1:200 000 (sediment polygons).

751   http://tupa.gtk.fi/paikkatieto/meta/maapera_200k.html (accessed 4.29.19).

752   Hanewinkel, M., Zhou, W., Schill, C., 2004. A neural network approach to identify forest

753   stands susceptible to wind damage. For. Ecol. Manag. 196, 227–243.

754   https://doi.org/10.1016/j.foreco.2004.02.056

755   Hart, E., Sim, K., Kamimura, K., Meredieu, C., Guyon, D., Gardiner, B., 2019. Use of

756   machine learning techniques to model wind damage to forests. Agric. For. Meteorol.

757   265, 16–29. https://doi.org/10.1016/j.agrformet.2018.10.022

758   Hastie, T., Tibshirani, R., Friedman, J., 2009. The elements of statistical learning, 2nd ed,

34

759   Springer Series in Statistics. Springer-Verlag New York.

760   Hijmans, R.J., 2017. raster: Geographic Data Analysis and Modeling. R package version

761   2.6-7. https://CRAN.R-project.org/package=raster.

762   Hijmans, R.J., Phillips, S., Leathwick, J., Elith, J., 2017. dismo: Species Distribution

763   Modeling. R package version 1.1-4. https://CRAN.R-project.org/package=dismo.

764   Honkaniemi, J., Lehtonen, M., Väisänen, H., Peltola, H., 2017. Effects of wood decay by

765   Heterobasidion annosum on the vulnerability of Norway spruce stands to wind

766   damage: a mechanistic modelling approach. Can. J. For. Res. 47, 777–787.

767   https://doi.org/10.1139/cjfr-2016-0505

768   Hosmer, D.W., Lemeshow, S., Strudivant, R.X., 2013. Applied Logistic Regression, 3rd ed.

769   John Wiley & Sons, New York.

770   Ikonen, V.-P., Kilpeläinen, A., Zubizarreta-Gerendiain, A., Strandman, H., Asikainen, A.,

771   Venäläinen, A., Kaurola, J., Kangas, J., Peltola, H., 2017. Regional risks of wind

772   damage in boreal forests under changing management and climate projections. Can.

773   J. For. Res. 47, 1632–1645. https://doi.org/10.1139/cjfr-2017-0183

774   Kabir, E., Guikema, S., Kane, B., 2018. Statistical modeling of tree failures during storms.

775   Reliab. Eng. Syst. Saf. 177, 68–79. https://doi.org/10.1016/j.ress.2018.04.026

776   Kamimura, K., Gardiner, B., Dupont, S., Guyon, D., Meredieu, C., 2015. Mechanistic and

777   statistical approaches to predicting wind damage to individual maritime pine (Pinus

778   pinaster) trees in forests. Can. J. For. Res. 46, 88–100. https://doi.org/10.1139/cjfr-

779   2015-0237

780   Korhonen, K.T., 2016. National forest inventories : Assessment of wood availability and use :

781   Finland, in: Vidal, C., Alberdi, I., Hernández, L., Redmond, J.J. (Eds.), National

782   Forest Inventories : Assessment of Wood Availability and Use. Springer International

783   Publishing, Switzerland, pp. 369–384.

784   Korhonen, K.T., Ihalainen, A., Ahola, A., Heikkinen, J., Henttonen, H.M., Hotanen, J.-P.,

785   Nevalainen, S., Pitkänen, J., Strandström, M., Viiri, H., 2017. Suomen metsät 2009–

786   2013 ja niiden kehitys 1921–2013 (No. 59/2017), Luonnonvara- ja biotalouden

35

787   tutkimus. Natural Resources Institute Finland (Luke).

788   Kuuluvainen, T., 2002. Disturbance dynamics in boreal forests: defining the ecological basis

789   of restoration and management of biodiversity. Silva Fenn. 36, 5–11.

790   Laapas, M., Lehtonen, I., Venäläinen, A., Peltola, H.M., 2019. The 10-Year Return Levels of

791   Maximum Wind Speeds under Frozen and Unfrozen Soil Forest Conditions in

792   Finland. Climate 7, 62. https://doi.org/10.3390/cli7050062

793   Lanquaye-Opoku, N., Mitchell, S.J., 2005. Portability of stand-level empirical windthrow risk

794   models. For. Ecol. Manag. 216, 134–148.

795   https://doi.org/10.1016/j.foreco.2005.05.032

796   Lohmander, P., Helles, F., 1987. Windthrow probability as a function of stand characteristics

797   and shelter. Scand. J. For. Res. 2, 227–238.

798   https://doi.org/10.1080/02827588709382460

799   Mäkisara, K., Katila, M., Peräsaari, J., 2019. The Multi-Source National Forest Inventory of

800   Finland - methods and results 2015 (No. 8/2019), Natural Resources and

801   Bioeconomy Studies. Natural Resources Institute Finland (Luke).

802   Mäkisara, K., Katila, M., Tomppo, E., 2016. The Multi-Source National Forest Inventory of

803   Finland – methods and results 2013 (No. 10/2016), Natural Resources and

804   Bioeconomy Studies. Natural Resources Institute Finland (Luke).

805   Mattila, U., Nuutinen, T., 2007. Assessing the incidence of butt rot in Norway spruce in

806   southern Finland. Silva Fenn. 41. https://doi.org/10.14214/sf.473

807   Mitchell, S.J., 2013. Wind as a natural disturbance agent in forests: a synthesis. For. Int. J.

808   For. Res. 86, 147–157. https://doi.org/10.1093/forestry/cps058

809   Müller, M.M., Henttonen, H.M., Penttilä, R., Kulju, M., Helo, T., Kaitera, J., 2018. Distribution

810   of Heterobasidion butt rot in northern Finland. For. Ecol. Manag. 425, 85–91.

811   https://doi.org/10.1016/j.foreco.2018.05.047

812   Nakou, A., Sauter, U.H., Kohnle, U., 2016. Improved models of harvest-induced bark

813   damage. Ann. For. Sci. 73, 233–246. https://doi.org/10.1007/s13595-015-0530-5

814   Narendra, P.M., Goldberg, M., 1980. Image Segmentation with Directed Trees. IEEE Trans.

36

815   Pattern Anal. Mach. Intell. PAMI-2, 185–191.

816   https://doi.org/10.1109/TPAMI.1980.4766999

817   Nicoll, B.C., Gardiner, B.A., Rayner, B., Peace, A.J., 2006. Anchorage of coniferous trees in

818   relation to species, soil type, and rooting depth. Can. J. For. Res. 36, 1871–1883.

819   NLS, 2018. Topographic Database https://www.maanmittauslaitos.fi/en/maps-and-spatial-

820   data/expert-users/product-descriptions/topographic-database.

821   Pebesma, E.J., Bivand, R.S., 2005. Classes and methods for spatial data in R (No. 5 (2),

822   https://cran.r-project.org/doc/Rnews/), R News.

823   Pekkarinen, A., 2002. Image segment-based spectral features in the estimation of timber

824   volume. Remote Sens. Environ. 82, 349–359. https://doi.org/10.1016/S0034-

825   4257(02)00052-4

826   Peltola, H., Ikonen, V.-P., Gregow, H., Strandman, H., Kilpeläinen, A., Venäläinen, A.,

827   Kellomäki, S., 2010. Impacts of climate change on timber production and regional

828   risks of wind-induced damage to forests in Finland. For. Ecol. Manag. 260, 833–845.

829   https://doi.org/10.1016/j.foreco.2010.06.001

830   Peltola, H., Kellomäki, S., Väisänen, H., Ikonen, V.-P., 1999. A mechanistic model for

831   assessing the risk of wind and snow damage to single trees and stands of Scots

832   pine, Norway spruce, and birch. Can. J. For. Res. 29, 647–661.

833   https://doi.org/10.1139/x99-029

834   R Core Team, 2018. R: A language and environment for statistical computing. R Foundation

835   for Statistical Computing, Vienna, Austria. https://www.R-project.org/.

836   Reyer, C.P.O., Bathgate, S., Blennow, K., Borges, J.G., Bugmann, H., Delzon, S., Faias,

837   S.P., Garcia-Gonzalo, J., Gardiner, B., Gonzalez-Olabarria, J.R., Gracia, C.,

838   Hernández, J.G., Kellomäki, S., Kramer, K., Lexer, M.J., Lindner, M., Maaten, E. van

839   der, Maroschek, M., Muys, B., Nicoll, B., Palahi, M., Palma, J.H., Paulo, J.A., Peltola,

840   H., Pukkala, T., Rammer, W., Ray, D., Sabaté, S., Schelhaas, M.-J., Seidl, R.,

841   Temperli, C., Tomé, M., Yousefpour, R., Zimmermann, N.E., Hanewinkel, M., 2017.

842   Are forest disturbances amplifying or canceling out climate change-induced

37

843   productivity changes in European forests? Environ. Res. Lett. 12, 034027.

844   https://doi.org/10.1088/1748-9326/aa5ef1

845 Robin, X., Turck, N., Hainard, A., Tiberti, N., Lisacek, F., Sanchez, J.-C., Müller, M., 2011.

846   pROC: an open-source package for R and S+ to analyze and compare ROC curves.

847   BMC Bioinformatics 12, 77. https://doi.org/10.1186/1471-2105-12-77

848 Saarinen, N., Vastaranta, M., Honkavaara, E., Wulder, M.A., White, J.C., Litkey, P.,

849   Holopainen, M., Hyyppä, J., 2016. Using multi-source data to map and model the

850   predisposition of forests to wind disturbance. Scand. J. For. Res. 31, 66–79.

851   https://doi.org/10.1080/02827581.2015.1056751

852 Schelhaas, M.-J., Nabuurs, G.-J., Schuck, A., 2003. Natural disturbances in the European

853   forests in the 19th and 20th centuries. Glob. Change Biol. 9, 1620–1633.

854   https://doi.org/10.1046/j.1365-2486.2003.00684.x

855 Schindler, D., Grebhan, K., Albrecht, A., Schönborn, J., 2009. Modelling the wind damage

856   probability in forests in Southwestern Germany for the 1999 winter storm 'Lothar.' Int.

857   J. Biometeorol. 53, 543–554. https://doi.org/10.1007/s00484-009-0242-3

858 Schindler, D., Jung, C., Buchholz, A., 2016. Using highly resolved maximum gust speed as

859   predictor for forest storm damage caused by the high-impact winter storm Lothar in

860   Southwest Germany. Atmospheric Sci. Lett. 17, 462–469.

861   https://doi.org/10.1002/asl.679

862 Schmidt, M., Hanewinkel, M., Kändler, G., Kublin, E., Kohnle, U., 2010. An inventory-based

863   approach for modeling single-tree storm damage — experiences with the winter

864   storm of 1999 in southwestern Germany. Can. J. For. Res. 40, 1636–1652.

865   https://doi.org/10.1139/X10-099

866 Seidl, R., Rammer, W., 2017. Climate change amplifies the interactions between wind and

867   bark beetle disturbances in forest landscapes. Landsc. Ecol. 32, 1485–1498.

868   https://doi.org/10.1007/s10980-016-0396-4

869 Seidl, R., Schelhaas, M.-J., Lexer, M.J., 2011. Unraveling the drivers of intensifying forest

870   disturbance regimes in Europe. Glob. Change Biol. 17, 2842–2852.

38

871   https://doi.org/10.1111/j.1365-2486.2011.02452.x

872   Seidl, R., Schelhaas, M.-J., Rammer, W., Verkerk, P.J., 2014. Increasing forest disturbances

873   in Europe and their impact on carbon storage. Nat. Clim. Change 4, 806–810.

874   https://doi.org/10.1038/nclimate2318

875   Seidl, R., Thom, D., Kautz, M., Martin-Benito, D., Peltoniemi, M., Vacchiano, G., Wild, J.,

876   Ascoli, D., Petr, M., Honkaniemi, J., Lexer, M.J., Trotsiuk, V., Mairota, P., Svoboda,

877   M., Fabrika, M., Nagel, T.A., Reyer, C.P.O., 2017. Forest disturbances under climate

878   change. Nat. Clim. Change 7, 395–402. https://doi.org/10.1038/nclimate3303

879   Suvanto, S., Henttonen, H.M., Nöjd, P., Mäkinen, H., 2018. High-resolution topographical

880   information improves tree-level storm damage models. Can. J. For. Res. 48, 721–

881   728. https://doi.org/10.1139/cjfr-2017-0315

882   Suvanto, S., Henttonen, H.M., Nöjd, P., Mäkinen, H., 2016. Forest susceptibility to storm

883   damage is affected by similar factors regardless of storm type: Comparison of

884   thunder storms and autumn extra-tropical cyclones in Finland. For. Ecol. Manag. 381,

885   17–28. https://doi.org/10.1016/j.foreco.2016.09.005

886   Tomppo, E., Haakana, M., Katila, M., Peräsaari, J., 2008. Multi-Source National Forest

887   Inventory: Methods and Applications, Managing Forest Ecosystems. Springer

888   Netherlands.

889   Tomppo, E., Heikkinen, J., Henttonen, H.M., Ihalainen, A., Katila, M., Mäkelä, H.,

890   Tuomainen, T., Vainikainen, N., 2011. Designing and Conducting a Forest Inventory -

891   case: 9th National Forest Inventory of Finland, Managing Forest Ecosystems.

892   Springer Netherlands.

893   Valinger, E., Fridman, J., 2011. Factors affecting the probability of windthrow at stand level

894   as a result of Gudrun winter storm in southern Sweden. For. Ecol. Manag. 262, 398–

895   403. https://doi.org/10.1016/j.foreco.2011.04.004

896   Valinger, E., Fridman, J., 1997. Modelling probability of snow and wind damage in Scots

897   pine stands using tree characteristics. For. Ecol. Manag. 97, 215–222.

898   https://doi.org/10.1016/S0378-1127(97)00062-5

39

899   Valinger, E., Kempe, G., Fridman, J., 2014. Forest management and forest state in southern

900   Sweden before and after the impact of storm Gudrun in the winter of 2005. Scand. J.

901   For. Res. 29, 466–472. https://doi.org/10.1080/02827581.2014.927528

902   Venäläinen, A., Laapas, M., Pirinen, P., Horttanainen, M., Hyvönen, R., Lehtonen, I., Junila,

903   P., Hou, M., Peltola, H.M., 2017. Estimation of the high-spatial-resolution variability in

904   extreme wind speeds for forestry applications. Earth Syst. Dyn. 8, 529–545.

905   https://doi.org/10.5194/esd-8-529-2017

906   Wallentin, C., Nilsson, U., 2014. Storm and snow damage in a Norway spruce thinning

907   experiment in southern Sweden. For. Int. J. For. Res. 87, 229–238.

908   https://doi.org/10.1093/forestry/cpt046

909   Wand, M., 2015. KernSmooth: Functions for Kernel Smoothing Supporting Wand & Jones

910   (1995), R package version 2.23-15. https://CRAN.R-

911   project.org/package=KernSmooth.

912   Wood, S., 2017. Generalized Additive Models: An Introduction with R, Second Edition, 2nd

913   edition. ed.

914   Wood, S.N., 2011. Fast stable restricted maximum likelihood and marginal likelihood

915   estimation of semiparametric generalized linear models. J. R. Stat. Soc. Ser. B Stat.

916   Methodol. 73, 3–36.

917   Wood, S.N., Scheipl, F., 2017. gamm4: Generalized Additive Mixed Models using "mgcv"

918   and "lme4". R package version 0.2-5. https://CRAN.R-project.org/package=gamm4.

919

Supplementary materials

920

921   S1. The damage density ratio variable

922   S2. GAM model results

923   S3. BRT parameter tuning

924   S4. GLM variance-covariance matrix

41